On the Heating of the Slow Solar-Wind by Imbalanced Alfvén-Wave Turbulence from 0.06 au to 1 au: *Parker Solar Probe* and *Solar Orbiter* observations

Sofiane Bourouaine,[1] Jean C. Perez,[1] Benjamin D. G. Chandran,[2] Vamsee K. Jagarlamudi,[3] Nour E. Raouafi,[3] and Jasper S. Halekas[4]

[1] *Department of Aerospace, Physics and Space Sciences, Florida Institute of Technology, Melbourne, Florida, 32901, USA.*
[2] *Space Science Center, University of New Hampshire, Durham, NH, 03824, USA.*
[3] *Johns Hopkins University Applied Physics Laboratory, Laurel, MD 20723, USA.*
[4] *Department of Physics and Astronomy, University of Iowa, Iowa City, IA 52242, USA*

ABSTRACT

In this work we analyze plasma and magnetic field data provided by the Parker Solar Probe (*PSP*) and Solar Orbiter (*SO*) missions to investigate the radial evolution of the heating of Alfvénic slow wind (ASW) by imbalanced Alfvén-Wave (AW) turbulent fluctuations from 0.06 au to 1 au. in our analysis we focus on slow solar-wind intervals with highly imbalanced and incompressible turbulence (i.e., magnetic compressibility $C_B = \delta B/B \leq 0.25$, plasma compressibility $C_n = \delta n/n \leq 0.25$ and normalized cross-helicity $\sigma_c \geq 0.65$). First, we estimate the AW turbulent dissipation rate from the wave energy equation and find that the radial profile trend is similar to the proton heating rate. Second, we find that the scaling of the empirical AW turbulent dissipation rate Q_W obtained from the wave energy equation matches the scaling from the phenomenological AW turbulent dissipation rate Q_{CH09} (with $Q_{\mathrm{CH09}} \simeq 1.55 Q_W$) derived by Chandran & Hollweg (2009) based on the model of reflection-driven turbulence. Our results suggest that, as in the fast solar wind, AW turbulence plays a major role in the ion heating that occurs in incompressible slow-wind streams.

Keywords: TBA

1. INTRODUCTION

Previous in-situ measurements at heliocentric distances near and above 0.3 au revealed the existence of ubiquitous turbulent fluctuations throughout the interplanetary medium (see, e.g., the review of Bruno & Carbone (2013)). Most of these turbulent fluctuations have been found to be Alfvénic in nature and to propagate mainly outward from the Sun in the fast solar wind (Belcher & Davis 1971; Tu & Marsch 1995). Remote-sensing observations have also revealed the presence of Alfvén waves in the lower corona with sufficient energy to power the solar wind (De Pontieu et al. 2007; McIntosh et al. 2011). In addition, recent studies have investigated the heating of the solar wind by AWs turbulence using *PSP* measurements (Adhikari et al. 2021; Bandyopadhyay et al. 2023).

Generally, the solar wind is classified either as fast or slow wind with a typical speed of $V > 500$ km/s or $V \leq 500$ km/s, respectively. It is widely believed that Alfvén-Wave (AW) turbulence may substantially contribute to the heating and acceleration of the fast solar wind. The large-scale fluctuations may not be able to energize the solar wind directly, but they cascade to smaller-scale fluctuations via nonlinear processes (see, e.g., Verscharen et al. (2019)). At certain scales (near the ion scale), the turbulent fluctuations start to dissipate and provide thermal energy to the plasma. An important nonlinear cascade process occurs between two counter-propagating AWs (Howes & Nielson 2013), and one of the most likely sources of inward-propagating AWs is non-WKB reflection (Heinemann & Olbert 1980; Velli 1993; Hollweg & Isenberg 2007). Several solar-wind models (e.g., Cranmer et al. 2007; Verdini et al. 2010; Chandran et al. 2011; Usmanov et al. 2014; van der Holst et al. 2014) and direct numerical simulations of magnetohydrodynamic (MHD) turbulence (Perez & Chandran 2013; Dong et al. 2014; van Ballegooijen & Asgari-Targhi 2016, 2017; Chandran & Perez 2019; Shoda et al. 2019; Perez et al. 2021; Meyrand et al. 2023) have investigated

Corresponding author: Sofiane Bourouaine
sbourouaine@fit.edu

how AW turbulence and wave reflections might heat and accelerate the solar wind.

The fractional variations in the density and magnetic-field strength are often quite small in the fast solar wind, and the turbulent fluctuations in the fast solar wind are often observed to be imbalanced, in the sense that most of the turbulent fluctuations consist of Alfvén-wave-like fluctuations propagating away from the Sun in the plasma frame. Although some slow solar-wind streams are more balanced and compressible than the fast wind, other slow solar-wind streams have similar levels of compressibility and imbalance as the fast wind. This latter category of slow wind is referred to as the Alfvénic slow wind (ASW). Numerous intervals of ASW have been observed, for example, by the Parker Solar Probe (*PSP*; Raouafi et al. 2023a) (see also, Bale et al. 2019; Kasper et al. 2019; Chen et al. 2021; Bourouaine et al. 2020, 2022).

Although there is broad agreement that AW turbulence plays a key role in the origin of the fast solar wind, the origin of the slow solar wind is still a highly debated topic (Abbo et al. 2016). Recently, Raouafi et al. (2023b) argued that the solar wind is driven by jetting at the source. The magnetic reconnection at the corona naturally generates Alfvén waves that might heat and accelerate the solar wind at higher altitudes. Previous studies suggested that the solar origin of ASW comes from the boundaries of open coronal fields (D'Amicis & Bruno 2015; Bale et al. 2019), and non-Alfvénic slow wind could emanate from coronal streamers at the boundary of the heliospheric current sheet (Szabo et al. 2020; Chen et al. 2021).

Most previous studies of solar-wind heating by AW turbulence focused on the fast solar wind (e.g., Cranmer et al. 2009; Chandran et al. 2011; Adhikari et al. 2021; Bandyopadhyay et al. 2023). A notable exception to this was the recent study by Halekas et al. (2023), who quantified the radial profiles of the various contributions to the solar-wind energy flux in both the fast solar wind and slow solar wind.

In this paper, we analyze a set of measurements from *PSP* (for heliocentric distance $r = [0.06, 0.3]$ au) and Solar Orbiter (*SO*) (for $r = [0.3, 1]$ au) to investigate the heating of incompressible slow solar-wind streams by imbalanced AW turbulence. We use the steady-state electron and the proton energy equations to estimate the electron and proton heating rates. For the estimation of the AW turbulent dissipation rate, we use the fluctuation-energy equation in the steady state given in Perez et al. (2021). Our analysis differs from that of Halekas et al. (2023) in that we isolate the effects of AW dissipation and plasma heating, rather than quantifying the total plasma energization resulting from the combination of AW dissipation and the work done by AWs. In section 2, we describe our methodology and data analysis for the estimation of the plasma and turbulent parameters. The main results are presented in section 3. Finally, in section 4, we summarize and discuss our findings.

2. METHODOLOGY AND DATA ANALYSIS

In our analysis, we use plasma and field measurements from *PSP* and *SO*. The data from *SO* (from August 8 2022 to January 31 2023) are used to study the radial profile of the plasma heating rate and the AW turbulent heating rate between 0.3 au and 1 au. We use data from Encounters 2,4,5,6,7,9 and 10 of *PSP* for the analysis between 0.06 au and 0.3 au. These Encounters are chosen due to the availability of plasma density that is estimated through the quasi-thermal-noise (QTN) (Moncuquet et al. 2020).

2.1. *Selection of intervals*

In our analysis, we investigate the radial evolution of the solar-wind plasma as well as the AW turbulent dissipation rate. We divide *SO* and *PSP* data into 9 hours intervals, only intervals corresponding to 9-hours averaged solar-wind speed $V < 500$ km/s are initially considered. Both *SO* and *PSP* measure solar-wind plasma near the ecliptic; therefore, there will be occasions for some intervals with a mixed field polarity. To eliminate those intervals, we only consider intervals in which at least 70% of the instantaneous B_r values have the same sign, where B_r is the radial component of the magnetic field. The time duration of each interval is chosen to be $T = 9$ hours so that the large-scale part of the turbulence can be recovered. For those slow-wind selected intervals, the background (averaged) magnetic-field vector $\boldsymbol{B}_0$ is properly estimated. Then we estimate the turbulence parameters, such as the plasma compressibility, $C_n = \delta n_{\rm rms}/\langle n \rangle$; the magnetic compressibility, $C_B = \delta B_{\rm rms}/\langle |B| \rangle$; and the normalized cross helicity,

$$\sigma_c = \frac{\langle 2\delta \boldsymbol{V} \cdot \delta \boldsymbol{b} \rangle}{(\langle \delta V^2 \rangle + \langle \delta b^2 \rangle)}. \tag{1}$$

Here $\delta n_{\rm rms}$ and $\delta B_{\rm rms}$ are the root mean square of the fluctuating number density $n = n_e$ (here we assume $n_e \simeq n_p$, where n_e and n_p are the electron and proton density), and the magnetic field strength, respectively. The symbol $\langle \cdots \rangle$ denotes an average over the time period T for each selected interval. The quantities $\delta \boldsymbol{V}$ and $\delta \boldsymbol{b}$ are the fluctuating bulk velocity and the fluctuating Alfvén velocity (i.e., $\delta \boldsymbol{b} = \delta \boldsymbol{B}/\sqrt{4\pi\rho_0}$, where ρ_0 is the proton mass density averaged over the time interval T.)
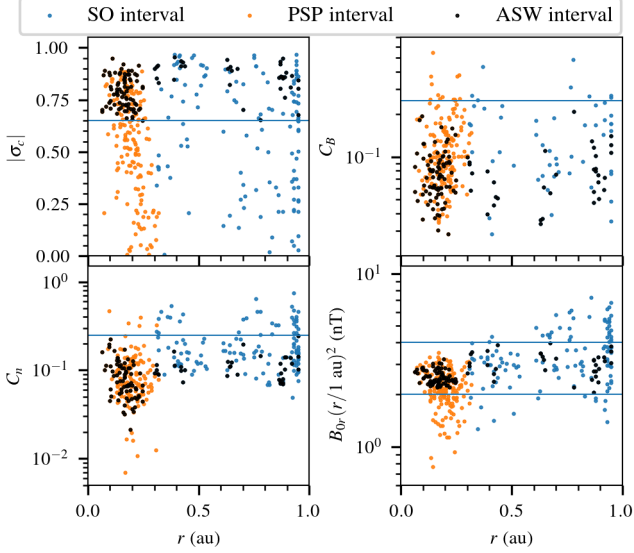
Figure 1. Top left panel: The normalized cross-helicity $|\sigma_c|$. Top right panel: The magnetic compressibility C_B. Bottom left panel: The plasma compressibility C_n. Bottom right panel: The quantity $B_{0r}(r/\,\text{au})^2$ in nT unit that is proportional to the magnetic field flux. The orange (blue) scatter points are the slow-wind *PSP* (*SO*) intervals with more than 70% of either sun outward or inward magnetic field polarity. The black dots correspond to the selected ASW intervals used for our analysis, i.e., intervals that satisfy; $C_B < 0.25$, $C_n < 0.25$, $|\sigma_c| > 0.65$ and that $B_{0r}(r/1\,\text{au})^2$ ranges between 2 nT and 4 nT.

These parameters allow us to select intervals of Alfvénic slow solar wind (ASW). We consider ASW intervals to be those intervals that are less compressible and where AW turbulence is imbalanced (i.e., by choosing $|\sigma_c| > 0.65$, $C_B \leq 0.25$ and $C_n \leq 0.25$). In Figure 1, we show a scatter plot for σ_c (upper left panel), C_B (upper right panel), and C_n (lower left panel) corresponding to all 9-hour slow-wind intervals satisfying the condition that more than 70% of the instantaneous B_r values within the interval have the same sign. Overall, about 60% of $|\sigma_c|$ values are higher than 0.65. Since we are interested in slow-wind intervals with AW turbulence, we apply the low-compressibility condition too such that $C_B < 0.25$ and $C_n < 0.25$. More than 70% of slow-wind intervals have $C_B < 0.25$ and $C_n < 0.25$. To study the evolution of the radial profile of heating and turbulent dissipation rates in ASW we apply another condition to the selected intervals, i.e., we only consider those intervals where the quantity $B_0(r/1\,\text{au})^2 \cos\psi = |B_{0r}|(r/1\,\text{au})^2$ (proportional to the magnetic flux) is between 2 and 4 nT, as indicated by the two horizontal lines in the lower right panel of Figure 1. Here ψ is the Parker angle that depends on the solar-wind speed and heliocentric distance r as

$\tan\psi = \Omega r/V$, where $\Omega = 2.7 \times 10^{-6}$ rad s^{-1} is the solar rotation frequency, and B_{0r} is the radial component of the averaged field $\boldsymbol{B}_0$. Overall, only $\simeq 28\%$ of the slow-wind intervals seen by *PSP* and SO (during the data period considered) satisfy the criteria of ASW.

3. RESULTS

3.1. *Radial profiles of plasma and turbulent parameters for ASW.*

Using the selected ASW intervals that fulfill all conditions stated above, we can now estimate the radial profiles of the electron density n, average proton temperature T_p, the strength of the average magnetic field $|\boldsymbol{B}_0|$, the energy densities of the anti-sunward (sunward) AWs $E_{\text{out}} = \rho_0 \langle \delta Z_{\text{out}}^2 \rangle /4$ ($E_{\text{in}} = \rho_0 \langle \delta Z_{\text{in}}^2 \rangle /4$), and the energy densities of the fluctuating Alfvén velocity $E_b = \rho_0 \langle \delta b^2 \rangle /2$ and bulk velocity $E_V = \rho_0 \langle \delta V^2 \rangle /2$. Here $\delta \boldsymbol{Z}_{\text{out}} = \delta \boldsymbol{V} - \delta \boldsymbol{b}$ ($\delta \boldsymbol{Z}_{\text{in}} = \delta \boldsymbol{V} + \delta \boldsymbol{b}$) if the background vector magnetic field is pointing outward from the sun. However, if the background field is pointing toward the sun then $\delta \boldsymbol{Z}_{\text{out}} = \delta \boldsymbol{V} + \delta \boldsymbol{b}$ ($\delta \boldsymbol{Z}_{\text{in}} = \delta \boldsymbol{V} - \delta \boldsymbol{b}$). All these quantities are plotted in Figure 2. Each quantity is fit to a power-law function $A_0(r/1\,\text{au})^{-\alpha}$ for *PSP* and *SO* separately. The fitting parameters are summarized in Table (1) below:

	PSP		*SO*	
X	A_0	α	A_0	α
n (cm^{-3})	10	-1.95	9.35	-1.8
B_0 (nT)	2.62	-1.90	4.12	-1.77
T_p (K)	6.5e4	-0.95	8.9e4	-0.9
T_e (K)	1.4e5	-0.5	-	-
E_b (J m^{-3})	2.6e-12	-3.15	4.6e-12	-3.12
E_V (J m^{-3})	1.8e-12	-3.23	3.11e-12	-3.17
E_{out} (J m^{-3})	3.95e-12	-3.20	7.12e-12	-3.18
E_{in} (J m^{-3})	5.52e-13	-3.10	6.10e-13	-2.60

Table 1. Fitting parameters A, α for each measured quantity $X = A_0(r/1\,\text{au})^{-\alpha}$ for Alfvénic slow-wind (ASW).

3.2. *Estimation of the proton and electron heating rates in ASW*

To estimate the empirical proton heating rate Q_p we use the fitting functions for the proton temperature T_p and the density n. This is to evaluate the derivatives with respect to r in the steady-state proton energy equation (see e.g., Cranmer et al. (2009))

$$\frac{3}{2}n^{5/3}k_B V_0 \frac{d}{dr}\left(\frac{T_p}{n^{2/3}}\right) = Q_p + \frac{3}{2}\nu_{ep}nk_B(T_e - T_p), \quad (2)$$
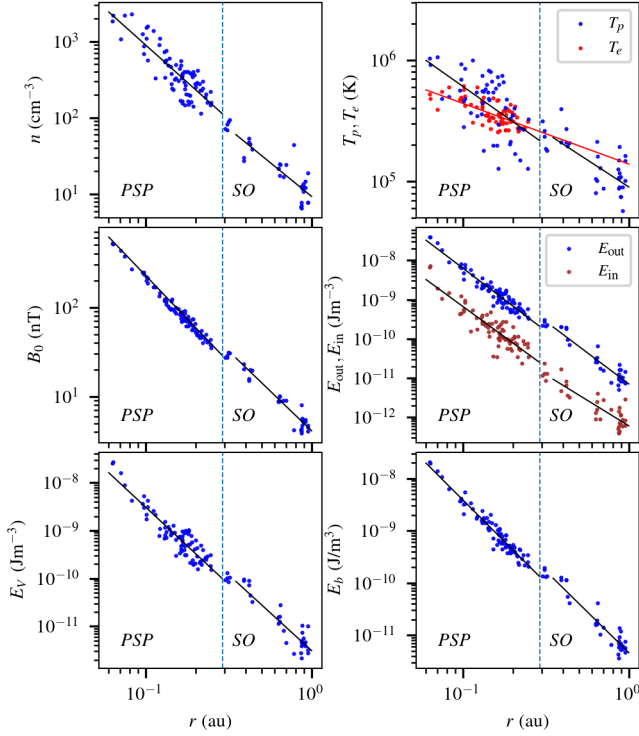
Figure 2. Top panels from left to right: The plasma density n and the proton temperature T_p. Middle panels from left to right: The strength of the average magnetic field B_0 and the energy densities of the anti-sunward E_{out} sunward E_{in} AWs. Bottom panels from left to right: The energy densities of the kinetic energy density E_V and the magnetic energy density E_b in velocity unit. All plotted as a function of the radial distance r.

where k_B is Boltzmann constant and ν_{ep} is the frequency of electron–proton Coulomb collisions. T_e is the electron temperature that is analyzed using only *PSP* data. We found that

$$T_e = 1.4 \times 10^5 \text{ k } (r/1 \text{ au})^{\alpha_e}, \tag{3}$$

with $\alpha_e = -0.5$. This radial profile of T_e will be used to estimate the electron heating rate from 0.06 au to 1 au. Here, V_0 corresponds to the mean solar-wind speed averaged over all ASW intervals, it is $V_0 = 370$ km/s for ASW *SO* intervals and $V_0 = 315$ km/s for ASW *PSP* intervals. The collision term in the r.h.s of Eq. (2) is insignificant but still calculated assuming two isotropic Maxwellian distributions for electrons and protons interacting with one another (Spitzer & Härm 1953). The frequency ν_{ep} is thus estimated from Cranmer et al. (2009)

$$\nu_{ep} \simeq 8.4 \times 10^{-9} \left(\frac{n}{2.5 \text{ cm}^{-3}} \right) \left(\frac{T_e}{10^5 \text{ K}} \right)^{-3/2} \text{ s}^{-1}. \tag{4}$$

Eq. (2) can be practically simplified by implementing the fitting functions $A_0(r/r_0)^{-\alpha}$ of n and T_p to evalu-

ate the derivatives with respect to r. Then, the proton heating rate Q_p is given by

$$Q_p = \frac{3}{2}nk_B \left[V_0 \left(\alpha_p - \frac{2}{3}\alpha_n \right) \frac{T_p}{r} - \nu_{pe} \left(T_e - T_p \right) \right], \tag{5}$$

where α_p and α_n are the exponents of the power-law fits of T_p and n, respectively. Similarly, the radial profile of the electron heating rate Q_e will be estimated by implementing power-law fits of T_e, and n into the following steady-state electron energy equation

$$\frac{3}{2}n^{5/3}k_B V_0 \frac{d}{dr} \left(\frac{T_e}{n^{2/3}} \right) = Q_e + \frac{3}{2}\nu_{ep}nk_B(T_p - T_e)$$
$$- \frac{1}{r^2}\frac{\partial}{\partial r}\left(q_{\parallel,e}r^2 \cos\psi \right). \tag{6}$$

Here $q_{\parallel,e}$ is the parallel electron heat flux. We estimate $q_{\parallel,e}$ based on the collisionless model (Hollweg 1974, 1976) as

$$q_{\parallel,e} = \frac{3}{2}\alpha_H n V_0 k_B T_e, \tag{7}$$

where α_H is a dimensionless parameter that is only known approximately. For fast wind analysis Chandran et al. (2011) set $\alpha_H = 0.75$. In our analysis of ASW we evaluate Q_e for $\alpha_H = 0.5$, 0.75 and 0.90. In order to evaluate the derivative of the electron heat flux term in Eq. (6) we use the conservation of the magnetic field flux $B_0 r^2 \cos\psi = $ constant and the fitting functions of T_e, n and B_0 that we measured. The electron heating rate is then

$$Q_e = \frac{3}{2}nk_B \left[V_0 \left(\alpha_e - \frac{2}{3}\alpha_n \right) \frac{T_e}{r} - \nu_{ep}(T_p - T_e) \right]$$
$$+ \frac{q_{\parallel,e}}{r}\cos\psi \left(\alpha_n + \alpha_e - \alpha_B \right) \tag{8}$$

Figure 3 shows the empirical values of Q_p and Q_e estimated from *PSP* (at $r < 0.3$ au) and *SO* (at $r > 0.3$ au). We found that the fitting functions of the radial profiles proton rates are $Q_p = 0.83 \cdot 10^{-17}(r/1 \text{ au})^{-3.92}$ J m^{-3} s^{-1} ($Q_p = 1.25 \cdot 10^{-17}(r/1 \text{ au})^{-3.66}$ J m^{-3} s^{-1}) at $r < 0.3$ au ($r > 0.3$ au) using *PSP* (*SO*). In Table (2) we show the electron heating rates for different values of α_H.

The proton heating rate needed for ASW is slightly less than the one for the fast solar wind, $Q_p^{fast} = 2.4 \cdot 10^{-17}(r/1 \text{ au})^{-3.8}$ J m^{-3} s^{-1} found by Hellinger et al. (2011) using *Helios* measurements.

It is worth-mentioning that formula given in Eq (7) with $\alpha_H = 0.5$, 0.75 and 0.9 guarantees that the conductive heating term is comparable in magnitude to the advective terms in Eq. (6) in our analysis.
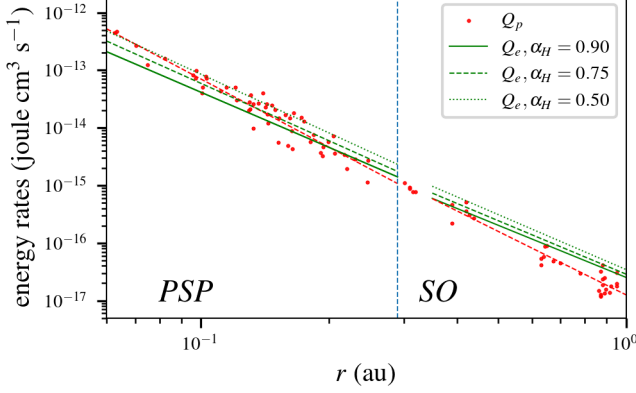
Figure 3. Red dots: Measured proton heating rate Q_p for ASW at $r < 0.3$ au ($r > 0.3$ au) using *PSP* (*SO*). Green lines: is the estimated electron heating rate Q_e for ASW at $r < 0.3$ au ($r > 0.3$ au) using $T_e = 1.4 \cdot 10^5 (r/1 \text{ au}))^{-0.5}$ (K) for $\alpha_H = 0.9$ (solid), $\alpha_H = 0.75$ (dashed) and $\alpha_H = 0.5$ (dotted).

(J m^{-3} s^{-1})	*PSP* ($r < 0.3$ au)	*SO* ($r > 0.3$ au)
$Q_e(\alpha_H = 0.9)$	$2.75 \cdot 10^{-17} \hat{r}^{-3.17}$	$2.52 \cdot 10^{-17} \hat{r}^{-3.00}$
$Q_e(\alpha_H = 0.75)$	$2.90 \cdot 10^{-17} \hat{r}^{-3.30}$	$2.87 \cdot 10^{-17} \hat{r}^{-3.10}$
$Q_e(\alpha_H = 0.5)$	$3.50 \cdot 10^{-17} \hat{r}^{-3.38}$	$3.44 \cdot 10^{-17} \hat{r}^{-3.17}$
Q_p	$0.83 \cdot 10^{-17} \hat{r}^{-3.92}$	$1.25 \cdot 10^{-17} \hat{r}^{-3.66}$

Table 2. The heating rates Q_e and Q_p for the Alfvénic slow wind (ASW). Here $\hat{r} = (r/1 \text{ au})$

3.3. *Estimation of turbulent dissipation rate Q_W in ASW*

To investigate the radial dissipation rate Q_W of the AW (imbalanced turbulence) in the slow-solar wind, we use the steady-state wave-energy equation given in Perez et al. (2021) but we account for the Parker spiral field geometry for the flux-tube, thus we have

$$\frac{d}{r^2 dr}\left[r^2 \cos\psi (F^{\text{out}} + F^{\text{in}})\right] = -Q_w$$
$$- E_b \frac{d}{r^2 dr}(V r^2 \cos\psi) - \eta V \xi_r \quad (9)$$

where $F^{\text{out}} = (V + V_A)E_{\text{out}}$ ($F^{\text{in}} = (V - V_A)E_{\text{in}}$) is the flux density of the anti-sunward (sunward) AWs, $\eta = -\cos\psi dB_0/(B_0 dr)$, $\xi_r = E_V - E_b$ is the average residual energy density. Now, we introduce the measured power-law fitting functions of $E_{\text{out}} \propto r^{\alpha_{\text{out}}}$, $E_{\text{in}} \propto r^{\alpha_{\text{in}}}$, $|B_0| \propto r^{\alpha_B}$ and $n \propto r^{-\alpha_n}$ to estimate the turbulent heating rate Q_W from Eq. (9). The power-law functions and the magnetic-field flux conservation will allow us to simplify the derivatives in Eq. (9). Also, by considering that solar wind speed is nearly constant we now can use the
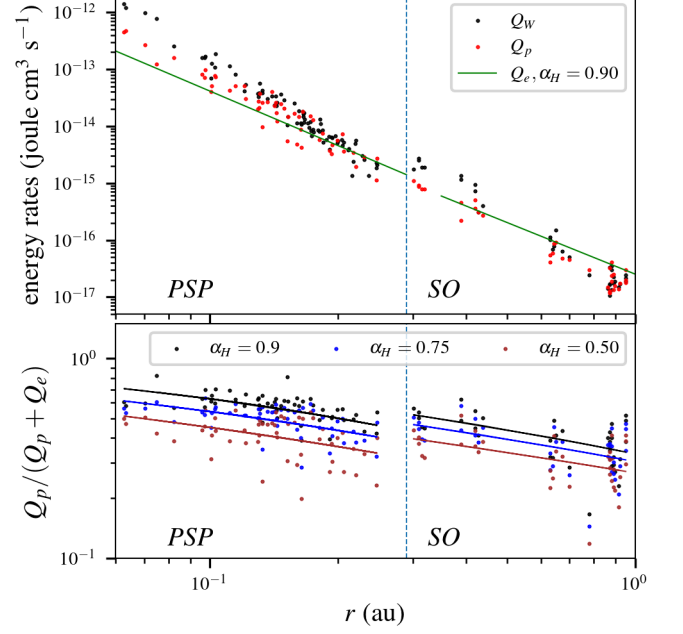

Figure 4. Top panel: Black dots are the estimated turbulent dissipation rate Q_W from Eq. (10) for ASW intervals for $r < 0.3$ au ($r > 0.3$ au) using *PSP* (*SO*). Red dots represent the proton heating rate Q_p for ASW. Solid green line represents the estimated electron heating rate Q_e when $\alpha_H = 0.9$. Bottom panel: proton-to-total heating ratio versus heliocentric distance when $\alpha_H = 0.9$, $\alpha_H = 0.75$ and $\alpha_H = 0.5$, and the solid lines are the same ratio obtained from the power-law fits of Q_p and Q_e.

following expression of Q_W as

$$Q_W = -\frac{V_0 \cos\psi}{r}\Big[C_{\text{out}}(\alpha_{\text{out}} - \alpha_B)E_{\text{out}} +$$
$$C_{\text{in}}(\alpha_{\text{in}} - \alpha_B)E_{\text{in}} - \alpha_B E_v\Big], \quad (10)$$

where $C_{\text{out}} = 1 + V_0/V_A$, $C_{\text{in}} = 1 - V_0/V_A$; and α_B, α_{out} and α_{in} are the the power-law fitting exponents of B_0, E_{out} and E_{in}, respectively.

In Figure 4, we plot the estimated Q_W (based on Eq. (10)) as a function of r using *PSP* (for $r < 0.3$ au) and *SO* (for $r > 0.3$ au) for ASW intervals. Interestingly enough, the trend of the turbulent dissipation rate Q_W for ASW follows the trend of the proton heating rate Q_p over the entire range of heliocentric distances r we studied. On average, the turbulent heating rate Q_W is about 1.5 times higher than the proton heating rates Q_p. The lower panel in Figure 4 shows the ratio $Q_p/(Q_p+Q_e)$ for $\alpha_H = 0.9$, 0.75 and $\alpha_H = 0.5$ as a function of r. Overall, It seems that the protons are more heated than electrons in ASW when $\alpha_H \gtrsim 0.9$. Here we did not consider the collisional Spitzer-Härm (SH) electron heat flux as the majority of the observed electron heat flux near-Sun

region using *PSP* data lie below the SH limit (Halekas et al. 2021). Using SH heat flux in our analysis would lead to electron cooling instead of electron heating.

3.4. *Comparison with a phenomenological model of the heating rate in reflection-driven AW turbulence*

Dmitruk et al. (2002) derived a phenomenological turbulent heating rate for reflection-driven turbulence in coronal holes in the absence of background flow. They assumed that there is much more energy in waves propagating away from the Sun than waves propagating towards the Sun, and that the energy cascade timescale of Sunward-propagating waves is comparable to or shorter than their linear wave period. Chandran & Hollweg (2009) generalized this model to allow for the background flow of the solar wind, thereby taking into account the work done by the waves on the solar wind. The essence of these models is to balance the reflection rate of the produced sunward waves against the rate at which these waves cascade and dissipate via interactions with the anti-sunward waves. Chandran & Hollweg (2009) found that the turbulent heating rate in reflection-driven turbulence is

$$Q_{\mathrm{CH09}} = \frac{1}{4}\left(\frac{V + v_{\mathrm{A}}}{v_{\mathrm{A}}}\right)\left|\frac{\mathrm{d}v_{\mathrm{A}}}{\mathrm{d}r}\right|\rho\left(\delta z_{\mathrm{rms}}^{\mathrm{out}}\right)^2, \qquad (11)$$

where V is the solar-wind outflow velocity and v_A is Alfvén speed. We have estimated the turbulent energy dissipation rate Q_{CH09} using the ASW intervals selected for our analysis above. In Figure 5, we overplot the measured Q_{CH09} together with the estimated Q_W values obtained earlier from the turbulent energy equation (10). This figure shows that the two rates scale in a similar way with r and are comparable to each other with

$$Q_{\mathrm{CH09}} \simeq (1.55 \pm 0.45)Q_W, \qquad (12)$$

where the uncertainty ± 0.45 is the propagation error due to the power-law fits. This result provides good observational evidence supporting the reflection-driven turbulence model for turbulent heating in ASW, and is consistent with a related analysis using *PSP* data by Chen et al. (2020).

4. CONCLUSION AND DISCUSSION

In this work we analyzed plasma and magnetic-field data collected by *PSP* and *SO* to study the radial evolution of the plasma heating of the slow solar wind by incompressible Alfvénic turbulence. We selected intervals lasting approximately 9 hours in which at least 70% of the measured magnetic field has the same polarity – i.e., the same sign of B_r. We further restricted our analysis to comparatively incompressible intervals ($C_B < 0.25$
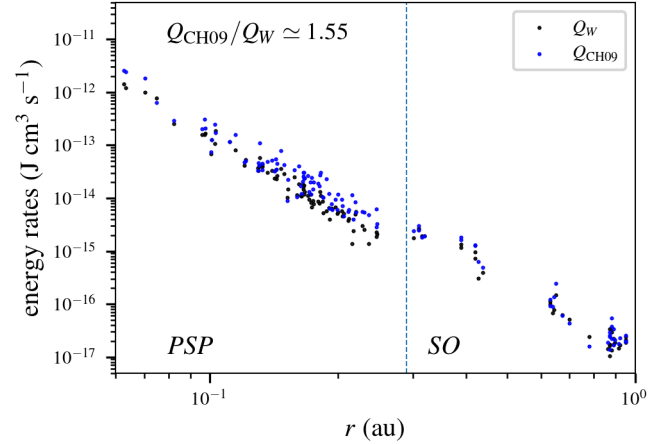

Figure 5. The estimated turbulent dissipation rate, Q_{CH09} from the turbulence reflection model of Chandran & Hollweg (2009) (blue dots) from Eq. (11) compared to the turbulent dissipation rate Q_W obtained from Eq. (10) (black dots). All measured using *PSP* for $r < 0.3$ au and *SO* at $r > 0.3$ au.

and $C_n < 0.25$) with a high degree of imbalance (i.e., $\sigma_c > 0.65$) — i.e., to ASW. We then analyzed those selected intervals to estimate the turbulent heating (dissipation) rate and the plasma (electron and proton) heating rate. We found that the radial profile of the proton heating rate in ASW correlates well with the turbulent heating rate Q_W which suggests that Alfvénic turbulence plays a major role in the heating of the protons in ASW, as it does in the fast solar wind. We also found that the measured AW turbulent heating rate agrees well with the phenomenological heating rate proposed by Chandran & Hollweg (2009) for reflection-driven AW turbulence.

Although our results show that AW turbulence can account for much of the heating of ASW between 0.06 au and 1 au, this does not mean that AW turbulence is the dominant mechanism for accelerating the ASW over this range of radii. Indeed, Halekas et al. (2023) used *PSP* data to examine the radial profiles of the various components of the solar-wind energy flux between $13R_\odot$ and $100R_\odot$. Because the solar-wind accelerates over this range of radii, the bulk-flow kinetic energy of the solar wind accounts for an increasing fraction of the total energy flux as r increases. For the slow solar wind, Halekas et al. (2023) showed that this radial increase is offset primarily by a decrease in the fraction of the energy flux carried by the electron enthalpy flux and heat flux. In other words, it is the electron enthalpy flux and heat flux that account for most of the acceleration of the slow solar wind between $13R_\odot$ and $100R_\odot$, not AW turbulence. Our results indicate that AW turbulence is likely the dom-

inant heating mechanism, at least in ASW. AW turbulence may heat mainly the protons in ASW through distinct possible heating mechanisms such as resonant-cyclotron heating by high-frequency ion-cyclotron waves (see e.g., Hollweg & Isenberg 2002) or by low-frequency AW turbulence (see, e.g., Bourouaine et al. 2008; Chandran et al. 2013; Bourouaine & Chandran 2013). The generation of the high-frequency waves in the solar wind could be triggered by low-frequency turbulence as shown in the numerical simulation work done by Squire et al. (2022).

REFERENCES

Abbo, L., Ofman, L., Antiochos, S. K., et al. 2016, SSRv, 201, 55

Adhikari, L., Zank, G. P., Zhao, L. L., Nakanotani, M., & Tasnim, S. 2021, A&A, 650, A16

Bale, S. D., Badman, S. T., Bonnell, J. W., et al. 2019, Nature, 576, 237

Bandyopadhyay, R., Meyer, C. M., Matthaeus, W. H., et al. 2023, ApJL, 955, L28

Belcher, J. W., & Davis, Jr., L. 1971, Journal of Geophysical Research, 76, 3534

Bourouaine, S., & Chandran, B. D. G. 2013, The Astrophysical Journal, 774, 96

Bourouaine, S., Marsch, E., & Vocks, C. 2008, ApJL, 684, L119

Bourouaine, S., Perez, J. C., Klein, K. G., et al. 2020, ApJL, 904, L30

Bourouaine, S., Perez, J. C., Raouafi, N. E., et al. 2022, ApJL, 932, L13

Bruno, R., & Carbone, V. 2013, Living Reviews in Solar Physics, 10, 2

Chandran, B. D. G., Dennis, T. J., Quataert, E., & Bale, S. D. 2011, The Astrophysical Journal, 743, 197

Chandran, B. D. G., & Hollweg, J. V. 2009, The Astrophysical Journal, 707, 1659

Chandran, B. D. G., & Perez, J. C. 2019, Journal of Plasma Physics, 85, doi:10.1017/S0022377819000540

Chandran, B. D. G., Verscharen, D., Quataert, E., et al. 2013, ApJ, 776, 45

Chen, C. H. K., Bale, S. D., Bonnell, J. W., et al. 2020, ApJS, 246, 53

Chen, C. H. K., Chandran, B. D. G., Woodham, L. D., et al. 2021, A&A, 650, L3

Cranmer, S. R., Matthaeus, W. H., Breech, B. A., & Kasper, J. C. 2009, ApJ, 702, 1604

Cranmer, S. R., van Ballegooijen, A. A., & Edgar, R. J. 2007, The Astrophysical Journal Supplement Series, 171, 520

D'Amicis, R., & Bruno, R. 2015, ApJ, 805, 84

De Pontieu, B., McIntosh, S. W., Carlsson, M., et al. 2007, Science, 318, 1574

Dmitruk, P., Matthaeus, W. H., Milano, L. J., et al. 2002, The Astrophysical Journal, 575, 571

Dong, Y., Verdini, A., & Grappin, R. 2014, ApJ, 793, 118

Halekas, J. S., Whittlesey, P. L., Larson, D. E., et al. 2021, A&A, 650, A15

Halekas, J. S., Bale, S. D., Berthomier, M., et al. 2023, ApJ, 952, 26

Heinemann, M., & Olbert, S. 1980, Journal of Geophysical Research, 85, 1311

Hellinger, P., Matteini, L., Štverák, Š., Trávníček, P. M., & Marsch, E. 2011, Journal of Geophysical Research (Space Physics), 116, A09105

Hollweg, J. V. 1974, J. Geophys. Res., 79, 3845

—. 1976, J. Geophys. Res., 81, 1649

Hollweg, J. V., & Isenberg, P. A. 2002, Journal of Geophysical Research (Space Physics), 107, 1147

—. 2007, Journal of Geophysical Research (Space Physics), 112, A08102

Howes, G. G., & Nielson, K. D. 2013, Physics of Plasmas, 20, 072302

Kasper, J. C., Bale, S. D., Belcher, J. W., et al. 2019, Nature, 576, 228

McIntosh, S. W., de Pontieu, B., Carlsson, M., et al. 2011, Nature, 475, 477

Meyrand, R., Squire, J., Mallet, A., & Chandran, B. D. G. 2023, arXiv e-prints, arXiv:2308.10389

Moncuquet, M., Meyer-Vernet, N., Issautier, K., et al. 2020, ApJS, 246, 44

Perez, J. C., & Chandran, B. D. G. 2013, The Astrophysical Journal, 776, 124

Perez, J. C., Chandran, B. D. G., Klein, K. G., & Martinović, M. M. 2021, Journal of Plasma Physics, 87, 905870218

Raouafi, N. E., Matteini, L., Squire, J., et al. 2023a, SSRv, 219, 8

Raouafi, N. E., Stenborg, G., Seaton, D. B., et al. 2023b, ApJ, 945, 28

Shoda, M., Suzuki, T. K., Asgari-Targhi, M., & Yokoyama, T. 2019, ApJL, 880, L2

Spitzer, L., & Härm, R. 1953, Physical Review, 89, 977

Squire, J., Meyrand, R., Kunz, M. W., et al. 2022, Nature Astronomy, 6, 715

Szabo, A., Larson, D., Whittlesey, P., et al. 2020, ApJS, 246, 47

Tu, C.-Y., & Marsch, E. 1995, Space Science Reviews, 73, 1

Usmanov, A. V., Goldstein, M. L., & Matthaeus, W. H. 2014, ApJ, 788, 43

van Ballegooijen, A. A., & Asgari-Targhi, M. 2016, The Astrophysical Journal, 821, 106

—. 2017, The Astrophysical Journal, 835, 10

van der Holst, B., Sokolov, I. V., Meng, X., et al. 2014, ApJ, 782, 81

Velli, M. 1993, Astronomy and Astrophysics, 270, 304

Verdini, A., Velli, M., Matthaeus, W. H., Oughton, S., & Dmitruk, P. 2010, The Astrophysical Journal Letters, 708, L116

Verscharen, D., Klein, K. G., & Maruca, B. A. 2019, Living Reviews in Solar Physics, 16, 5